Supporting Information

Synergistically Enhanced Co-Adsorption of HMF and Hydroxyl on Selenium and Oxygen Dual Vacancies in CeO_2-$CuNiSe_2$/NF for High-Efficiency HMF Electrooxidation

Junpu An†, Fan Yang*, Hongchen Liu, Kexin Wei, Chunhui Yu, Siyuan Sun, Yang Sun, Jiahui Liu, Xinyang Sun, Ruijing Feng and Yongfeng Li*

†Affiliation 1: State Key Laboratory of Heavy Oil Processing, China University of Petroleum, Beijing, 102249, China

* *Corresponding author: yangfan@cup.edu.cn (Fan Yang)*

* *Corresponding author: yfli@cup.edu.cn (Yongfeng Li)*

Electrochemical measurements

A standard H-cell, equipped with an FAA-3-50 membrane as the separator, was utilized for all electrochemical measurements with a CHI 760E electrochemical workstation. The system was configured with a three-electrode arrangement: a working electrode (geometric area: 1 cm^2), a platinum counter electrode, and a Hg/HgO reference electrode (internal electrolyte: 1 M KOH). The electrolyte for OER measurements consisted of 20 mL of 1 M KOH. For HMFOR experiments, the alkaline electrolyte was supplemented with 100 mM HMF. The potential measured against the Hg/HgO reference electrode was standardized to the reversible hydrogen electrode (RHE) scale using the following equation:

"E(RHE)=E(Hg/HgO) + 0.059*pH + 0.098"

The electrocatalytic activity for the hydrogen evolution reaction (HER), OER, and HMFOR was evaluated via LSV at a scan rate of 5 mV s^{-1}. The applied potential range was -0.6 to -1.4 V vs. Hg/HgO for HER and 0 to 0.8 V vs. Hg/HgO for OER and HMFOR.

The Tafel slope (b) was derived from the Tafel equation, $|\eta|=a + b \log |j|$, where η is the overpotential, a is a constant, and j is the current density.

Electrochemical impedance spectroscopy (EIS) characterization employed a fixed applied potential with frequencies sweeping from 100 kHz down to 0.1 Hz. A potential of 0.6 V vs. Hg/HgO was applied to the anode. For the determination of double-layer capacitance (C_{dl}), cyclic voltammetry (CV) scans were recorded at multiple scan rates (20-100 mV s^{-1}) within a non-Faradaic potential window. Subsequently, the ECSA was evaluated based on the C_{dl} values and the specific capacitance (C_s = 40 μF cm^{-2}) of an ideal flat electrode, according to the relationship ECSA = C_{dl} / C_s.

A flow cell setup was used to test the water electrolysis reaction. CeO_2-$CuNiSe_2$/NF with a size of 2 × 2 cm was employed as both the cathode and anode electrocatalyst, with a flow rate of 2.6 mL/min and a reservoir volume of 50 mL. No reference electrode is used in the flow cell. The water electrolysis activity in the

electrolyzer was investigated by applying a potential of 1.1-1.8 V.

High performance liquid chromatography analysis

Quantitative analysis of HMF and its derivatives was performed on a Shimadzu LC-10ADVP high-performance liquid chromatography (HPLC) system. For analysis, 20 μL aliquots were periodically withdrawn during constant-potential electrolysis, diluted 50 times with deionized water, and subjected to HPLC. The separation employed a C18 column with detection at 265 nm, employing a mobile phase of methanol and 5 mM ammonium formate solution (3:7) at a flow rate of 1.0 mL min^{-1}. Subsequent quantification relied on external calibration curves generated from pure standards, which provided the basis for calculating HMF conversion, FDCA selectivity, and FE.

Conversion (%) = (mol of HMF consumed) / (mol of initial HMF) × 100%

Selectivity (%) = (mol of FDCA yield) / (mol of initial HMF) × 100%

Faradic efficiency (%) = (mol of FDCA yield×6×F) / (total charge passed) × 100%

Here, F represents the Faraday constant (96,485 C mol^{-1}), and the factor 6 corresponds to the number of electrons transferred per molecule of FDCA formed.

Theoretical calculation

The density functional theory (DFT) computations in this work were carried out employing the CASTEP software package with spin polarization included. The exchange-correlation effects were described by the Perdew-Burke-Ernzerhof (PBE) functional under the generalized gradient approximation (GGA), augmented by Tkatchenko-Scheffler scheme for dispersion interactions. A plane-wave basis set with a cutoff energy of 450 eV was adopted, and k-space integration was performed using a 2×2×1 Monkhorst-Pack mesh. For structural relaxation, convergence criteria were set to stringent values of 1.0×10^{-5} eV/atom for energy, 0.01 eV/Å for maximum force, and 0.001 Å for maximum displacement. Convergence in the self-consistent field cycles was achieved when the energy difference was below 2×10^{-6} eV/atom, aided by a Fermi smearing width of 0.25 eV.

The adsorption energy was computed as $E_{ads} = E_{mol/sub} - (E_{mol} + E_{sub})$, where

$E_{mol/sub}$, E_{mol}, and E_{sub} correspond to the total energy of the adsorbed system, the energy of the free molecule in the gas phase, and the energy of the pristine catalyst surface, respectively.

1. Supplementary Figures

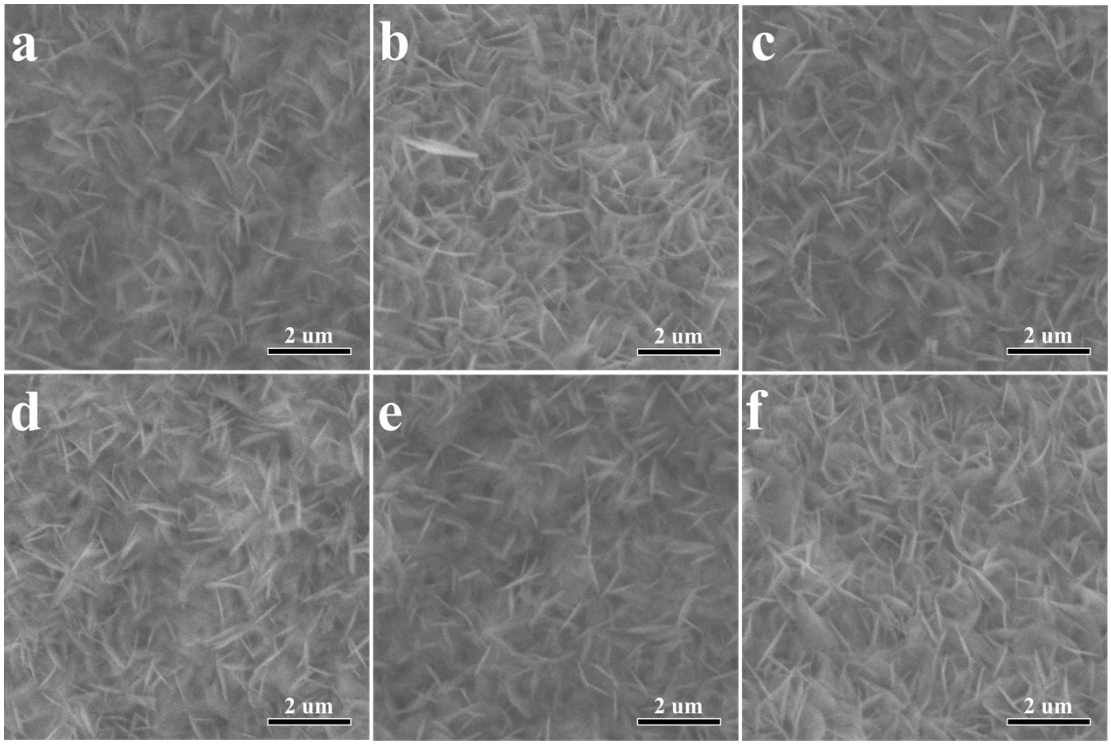

Figure S1. Scanning electron microscope (SEM) images: (a)Ce-CuNi precursors, (b) CeO_2/NF, (c) Cu_2Se/NF, (d) $NiSe_2$/NF, (e) $CuNiSe_2$/NF, and (f) CeO_2-$NiSe_2$/NF

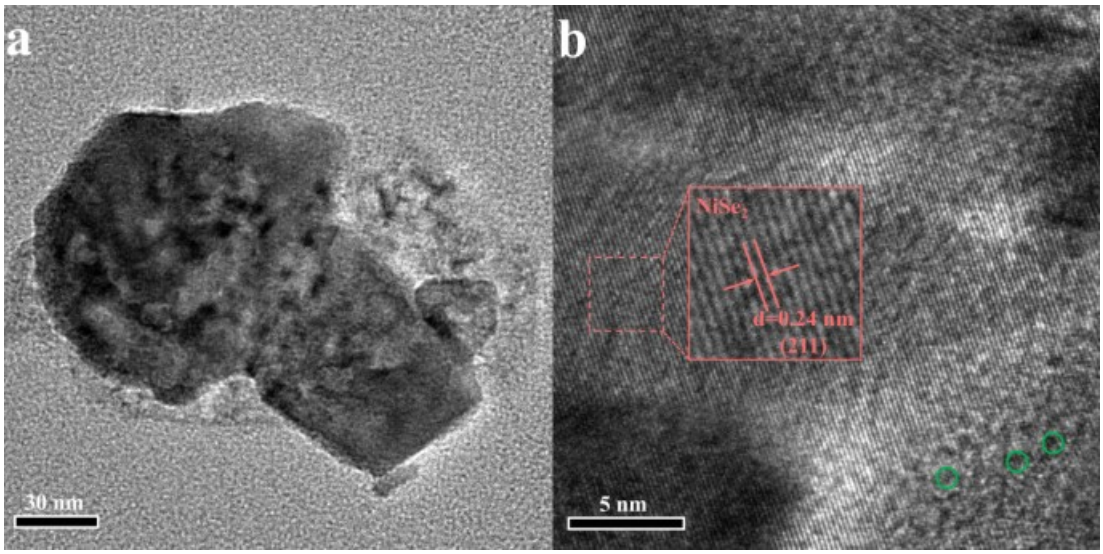

Figure S2. HR-TEM images of $NiSe_2$/NF (a and b).

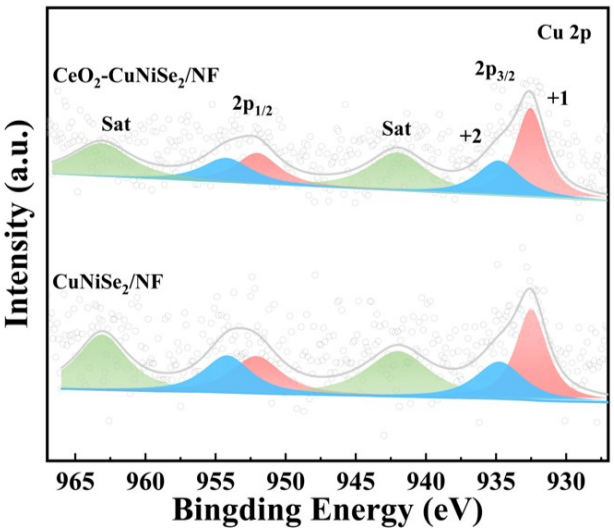

Figure S3. Cu 2p of CeO_2-$CuNiSe_2$/NF and $CuNiSe_2$/NF.

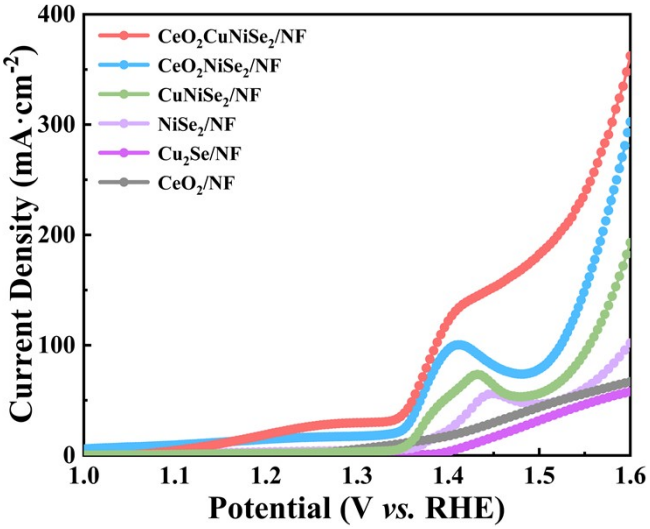

Figure S4. LSV curves of different samples in 1.0 M KOH.

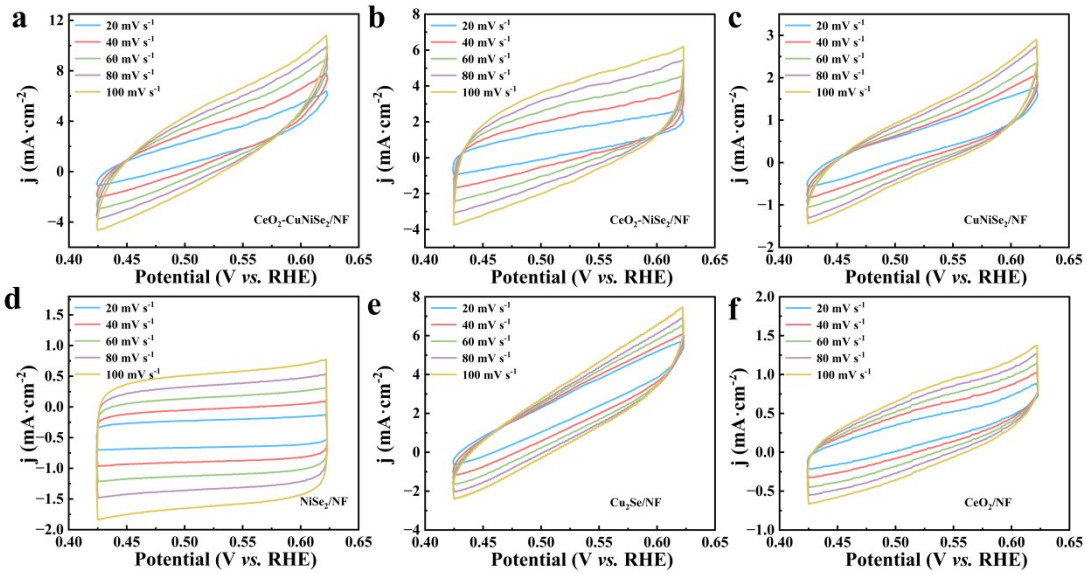

Figure S5. CV curves of (a) CeO_2-$CuNiSe_2$/NF, (b) CeO_2-$NiSe_2$/NF, (c) $CuNiSe_2$/NF, (d) $NiSe_2$/NF, (e) Cu_2Se/NF, and (f) CeO_2/NF at 20, 40, 60, 80, and 100 mV s^{-1} in 1 M KOH and 100 mM HMF.

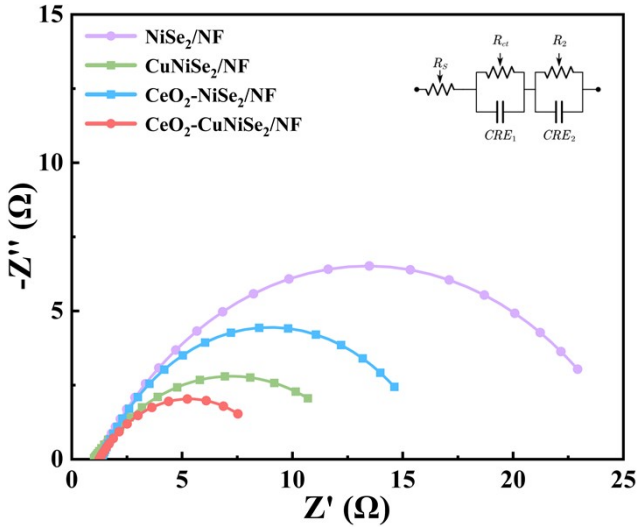

Figure S6. Nyquist plots (e) and Cdl values (e) of CeO_2-$CuNiSe_2$/NF, CeO_2-$NiSe_2$/NF, $CuNiSe_2$/NF, $NiSe_2$/NF, Cu_2Se/NF and CeO_2/NF.

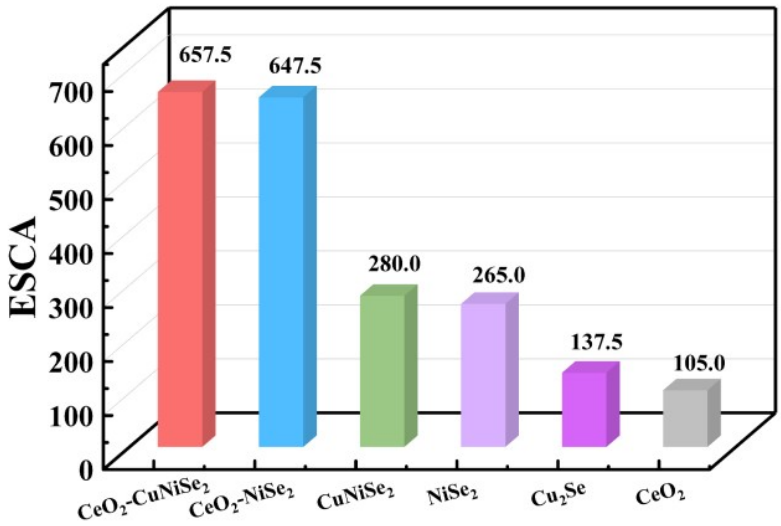

Figure S7. ECSA values of CeO_2-$CuNiSe_2$/NF, CeO_2-$NiSe_2$/NF, $CuNiSe_2$/NF, $NiSe_2$/NF, Cu_2Se/NF and CeO_2/NF

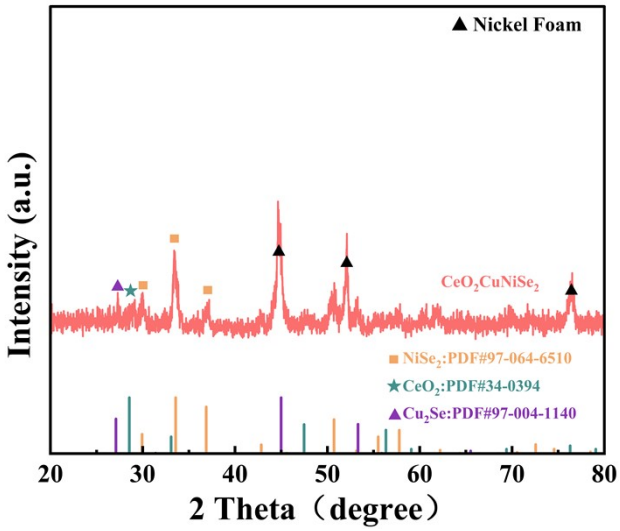

Figure S8. XRD pattern of CeO_2-$CuNiSe_2$/NF HMFOR after testing.

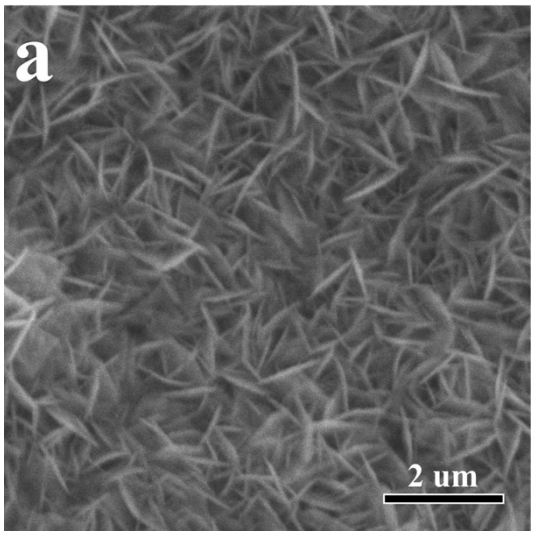

Figure S9. SEM of CeO_2-$CuNiSe_2$/NF HMFOR after testing.

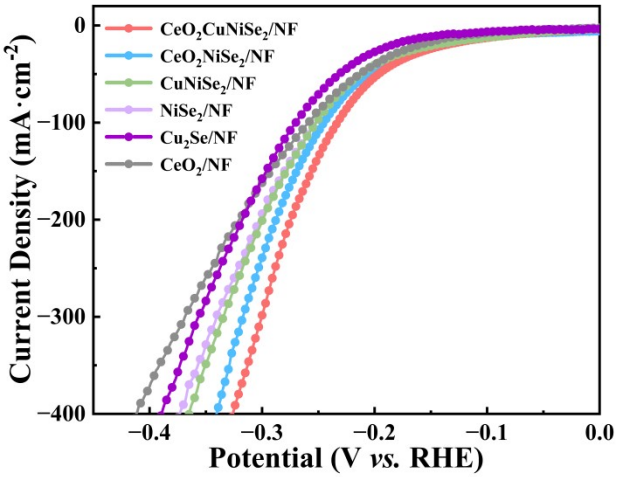

Figure S10. LSV curves of CeO_2-$CuNiSe_2$/NF, CeO_2-$NiSe_2$/NF, $CuNiSe_2$/NF, $NiSe_2$/NF, Cu_2Se/NF, and CeO_2/NF.

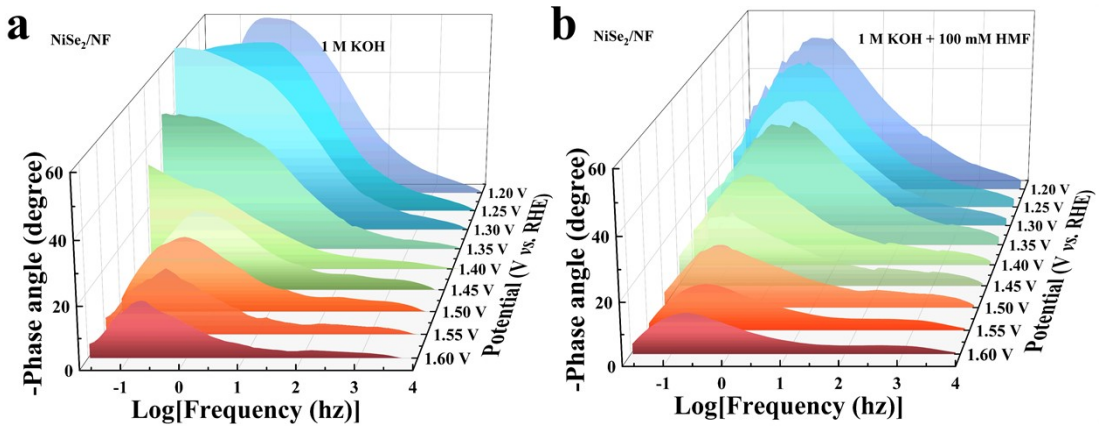

Figure S11. Bode plots of $NiSe_2$/NF (a and b)

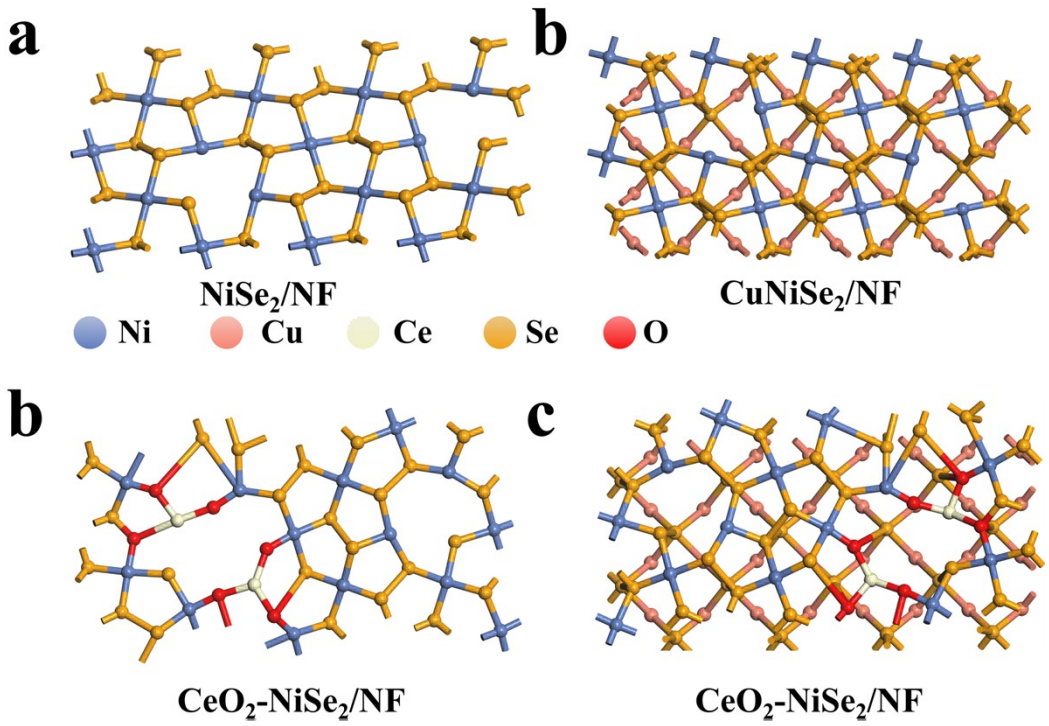

Figure S12. Top view of theoretical models of $NiSe_2$/NF, $CuNiSe_2$/NF, CeO_2-$NiSe_2$/NF, and CeO_2-$CuNiSe_2$/NF.

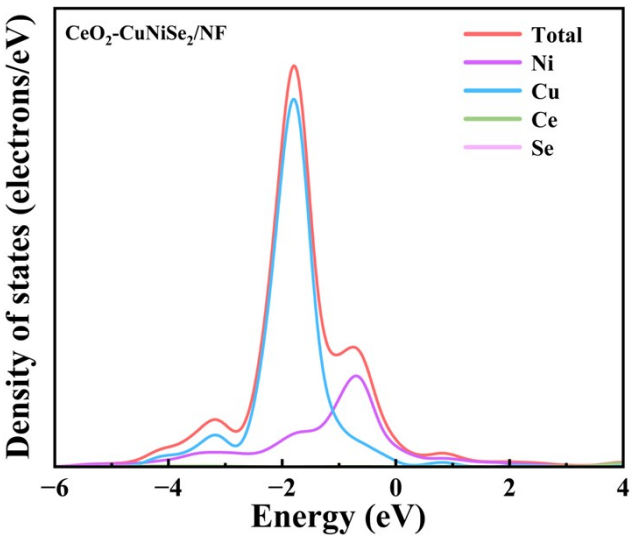

Figure S13.PDOS of CeO_2-$CuNiSe_2$/NF.

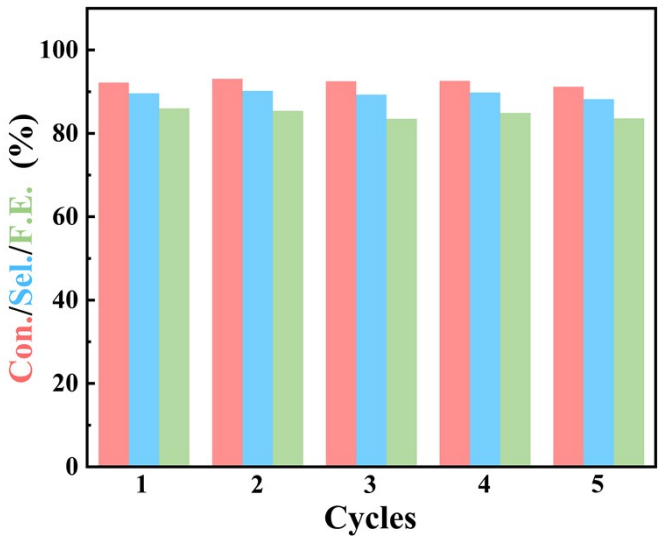

Figure S14.HMF conversion, FDCA selectivity, and FE of CeO_2-$CuNiSe_2$/NF during five consecutive electrolysis cycles in a flow cell.

Table S1. Elemental composition (weight percentage) obtained from ICP analysis.

Entry	Catalyst	Composition			
		Ce wt.%	Cu wt.%	Ni wt.%	Se wt.%
1	CeO_2-$CuNiSe_2$/NF	2.10	5.31	29.22	63.37
2	CeO_2-$CuNiSe_2$/NF after HMFOR test	3.36	6.90	32.41	57.33

Table S2. Comparison of HMFOR activity of CeO_2-$CuNiSe_2$/NF with other reported electrocatalysts

Catalysts	HMF Concentration（mM）	Voltage (V vs. RHE)	Current Density (mA cm^{-2})	Selec.（%）	Ref.
CeO_2-$CuNiSe_2$/NF	100	1.5	1230	98.3	This work
Pd-$NiCo_2O_4$	50	1.5	800	99.5	[1]
NiFe-LDH	100	1.5	300	98	[2]
$MoNi_4$/NF	100	1.5	90	98.7	[3]
Pt/CuO@CF	100			97.8	[4]
NiS_x/β-$Ni(OH)_2$/Ni	50	1.4	392	97.7	[5]
$CoNi_3S_2$@NF	50	1.4 1.45	368 497		[6]
CC@NiFeCe-LDH	50	1.47	100	93.3	[7]
NF/CoOOH@CeO_2	50	1.4	110	92.5	[8]
CuH_NWs@Ce:NiH_NSs	10	1.43	100	97.9	[9]
Ni-Cu/NF	50	1.4 1.5	500 1000		[10]
Pt/$Ni(OH)_2$	50	1.45	30		[11]
NiFe-1	100	1.425	700		[12]

Table S3. Comparison of cell voltage of CeO_2-$CuNiSe_2$/NF||CeO_2-$CuNiSe_2$/NF system for HER-HMFOR at 10 mA cm^{-2} with the reported electrocatalysts in two-electrode alkaline electrolytic cell.

Catalysts	HMF Concentration（mM）	Cell Voltage	Ref.
CeO_2-$CuNiSe_2$/NF	100	1.29V	This work
Rh-SA/NiFe NMLDH	50	1.32 V	[13]
Cu/Ni_3S_2-R	20	1.33 V	[14]
Cu_xS@NiCo-LDH	10	1.34 V	[15]
Ni_8PBA/CP	50	1.35 V	[16]
NF@Mo-$Ni_{0.85}Se$	10	1.41 V	[17]
NiCu NTs	20	1.48 V	[18]
Cu-NiFe PBA	100	1.48 V	[19]
$NiSe/NiO_x$	10	1.49 V	[20]

REFERENCES

1 X. Jiang, X. Ma, Y. Yang, Y. Liu, Y. Liu, L. Zhao, P. Wang, Y. Zhang, Y. Lin and Y. Wei, *Nano-Micro Lett.*, 2024, 16, 275.

2 W.-J. Liu, L. Dang, Z. Xu, H.-Q. Yu, S. Jin and G. W. Huber, *ACS Catal.*, 2018, 8, 5533–5541.

3 H. Liu, J. Xia, X. Liu, Y. Hu, M. Shakouri, H. Wu, M. Zhu, Y. Guo, J. Chen, H. Wang and Y. Wang, *ChemSusChem*, 2025, 18, e202401516.

4 J. Li, R. Qiu, S. Zhang, L. Peng, Y. Dong, Y. Jiang, Y. Li, N. Fang, J. Yu, J.-C. Dong, H. Zheng, L. Ding, J. Wan, I. Akpinar, J. Kuang, G. Chen, J. Ye, Y. Sun, L. Lin, S. Zheng, S. Yang, J. Li and J.-F. Li, *Adv. Mater.*, 2025, 37, 2417684.

5 C. Liu, X.-R. Shi, K. Yue, P. Wang, K. Zhan, X. Wang, B. Y. Xia and Y. Yan, *Adv. Mater.*, 2023, 35, 2211177.

6 Y. Sun, J. Wang, Y. Qi, W. Li and C. Wang, *Adv. Sci.*, 2022, 9, 2200957.

7 Y. Zhang, G. Hai, Z. Huang, Z. Liu, X. Huang and G. Wang, *Adv. Energy Mater.*, 2024, 14, 2401449.

8 P. Zhou, H. Pan, G. Hai, X. Liu, X. Huang and G. Wang, *J. Energy Chem.*, 2024, 98, 721–732.

9 G. Ren, B. Liu, L. Liu, M. Hu, J. Zhu, X. Xu, P. Jing, J. Wu and J. Zhang, *Inorg. Chem.*, 2023, 62, 12534–12547.

10 D. Chen, Y. Ding, X. Cao, L. Wang, H. Lee, G. Lin, W. Li, G. Ding and L. Sun, *Angew. Chem. Int. Ed.*, 2023, 62, e202309478.

11 B. Zhou, Y. Li, Y. Zou, W. Chen, W. Zhou, M. Song, Y. Wu, Y. Lu, J. Liu, Y. Wang and S. Wang, Angewandte Chemie International Edition, 2021, 60, 22908-22914.

12 C. Wang, Y. Wu, A. Bodach, M. L. Krebs, W. Schuhmann and F. Schüth, Angewandte Chemie International Edition, 2023, 62, e202215804.

13 L. Zeng, Y. Chen, M. Sun, Q. Huang, K. Sun, J. Ma, J. Li, H. Tan, M. Li, Y. Pan, Y. Liu, M. Luo, B. Huang and S. Guo, Journal of the American Chemical Society, 2023, 145, 17577-17587.

14 P. Xu, Z. Bao, Y. Zhao, L. Zheng, Z. Lv, X. Shi, H.-E. Wang, X. Fang and H. Zheng, Advanced Energy Materials, 2024, 14, 2303557.

15 X. Deng, X. Kang, M. Li, K. Xiang, C. Wang, Z. Guo, J. Zhang, X.-Z. Fu and J.-L. Luo, Journal of Materials Chemistry A, 2020, 8, 1138-1146.

16 N.-Y. Huang, B. Chu, D. Chen, B. Shao, Y.-T. Zheng, L. Li, X. Xiao and Q. Xu, Journal of the American Chemical Society, 2025, 147, 8832-8840.

17 C. Yang, C. Wang, L. Zhou, W. Duan, Y. Song, F. Zhang, Y. Zhen, J. Zhang, W. Bao, Y. Lu, D. Wang and F. Fu, Chemical Engineering Journal, 2021, 422, 130125.

18 L. Zheng, Y. Zhao, P. Xu, Z. Lv, X. Shi and H. Zheng, Journal of Materials Chemistry A, 2022, 10, 10181-10191.

19 Z. Liu, T. Xiao, X. Wu, C. Hu, X. F. Lu, H. Zhang, J. Zhang, X. Bao and P. Yuan, Applied Catalysis B: Environment and Energy, 2025, 378, 125601.

20 L. Gao, Z. Liu, J. Ma, L. Zhong, Z. Song, J. Xu, S. Gan, D. Han and L. Niu, Applied Catalysis B: Environmental, 2020, 261, 118235.